PG
Petroleum Geoscience

Research article

https://doi.org/10.1144/petgeo2022-059 | Vol. 29 | 2023 | petgeo2022-059

The role of organic carbon in the Southern Uplands-Down-Longford Terrane accretionary prism, Scotland and Ireland

J. Parnell[1]*, J. Armstrong[1], N.J.F. Blamey[2], A.J. Boyce[3], A. Schito[1] and D. Muirhead[1]

[1] School of Geosciences, University of Aberdeen, Aberdeen AB24 3UE, UK
[2] Department Earth Sciences, Western University, London, ON N6A 5B7, Canada
[3] Scottish Universities Environmental Research Centre, Rankine Avenue, East Kilbride G75 0QF, UK
JP, 0000-0002-5862-6933
* Correspondence: J.Parnell@abdn.ac.uk

Abstract: Carbonaceous shales in the Southern Uplands-Down-Longford Terrane accretionary prism had extremely high potential for hydrocarbon generation in the Lower Paleozoic. Structural thickening in the prism enhanced the rapid generation of oil. Shale horizons are separated by thick turbidites composed of low-permeability greywackes, so oil under high fluid pressure either pooled along shale bedding surfaces or migrated into fractured greywackes. Pooled oil became solidified to bitumen, which locally formed deposits on a scale of tonnes, mined as coal. The carbon-rich shale also sequestered large amounts of sulfur from seawater, which precipitated as pyrite firstly during early diagenesis, then further during fluid flow through the shale beds. The oil was also sulfur-bearing. Deformation focused on the shale beds during the evolution of the accretionary prism would have been closely related to the fluid flow which precipitated bitumen and sulfides. The palaeo-fluids were also anomalously rich in methane and hydrogen, similar to fluids venting from modern accretionary prisms.

Supplementary material: details of localities searched for coal in Lower Palaeozoic, Southern Uplands-Down-Longford Terrane (locations shown in Fig. 6) are available at https://doi.org/10.6084/m9.figshare.c.6691597

Received 11 August 2022; **revised** 1 May 2023; **accepted** 2 June 2023

Geological setting

The Ordovician–Silurian sedimentary package that constitutes the Southern Uplands-Down-Longford Terrane (SUDLT) was deposited and deformed on the northern margin of the Iapetus Ocean. The package is dominated by marine turbidites, with subordinate pelagic mudrocks and basalts. The mudrocks include a prominent unit of graptolitic black shales. The succession is structurally repeated by strike-parallel faults, which are the basis of an accretionary prism model for the package (Leggett 1980; Floyd 2001; Stone and Merriman 2004; Beamish *et al.* 2010). The black shales in the prism are of Llanvirn (Upper Ordovician) to Llandovery (Silurian) age, collectively termed the Moffat Shale (Floyd 1996). The imbricate structure of the SUDLT prism was facilitated by detachment on the Moffat Shale (Webb 1983; McCurry and Anderson 1989; Needham 2004). The black shale deposits of the Ordovician oceans had high hydrocarbon potential due to flourishing oil-rich algae (Reed *et al.* 1986; Makled *et al.* 2021), and abundant graptolite debris, with similar high hydrocarbon potential (Agapitov 2014; Luo *et al.* 2020). This study reports the evidence for hydrocarbon generation in the Southern Uplands-Down-Longford Terrane (Fig. 1).

The context for this assessment is a history of mining the Lower Paleozoic for so-called 'coal'. This was a carbonaceous substance in the shales which must have been emplaced post-deposition, as it cross-cuts the bedding (Whitty 1854). Some records may be exaggerated, but accounts of mining and selling fuel are indisputable, and as recently as the twentieth century the Commission of Inquiry into the Resources and Industries of Ireland (1921) suggested the possibility of including the fuel in briquettes.

The objectives of the study are:

(i) Measurement of the carbon content of selected localities in the Moffat Shale, and determination of a mean value for the richer beds.
(ii) Reconstruction of the original carbon content before hydrocarbon generation and low-grade metamorphism.
(iii) Assessment of burial history and likely hydrocarbon generation history within the context of accretionary prism construction.
(iv) Petrographic study of the distribution of hydrocarbon residues.
(v) Collation of supporting information on attempts to mine 'coal' in the Ordovician–Silurian rocks of the prism.
(vi) Measurement of sulfur isotope data in pyrite in the Moffat Shale as an indicator of fluid sources.

Methodology

Petrographic studies were performed at the University of Aberdeen ACEMAC Facility using a Zeiss Gemini field emission gun scanning electron microscope (FEG-SEM) on polished blocks of the marble. Samples were carbon coated and analysed at 20 kv, with a working distance of 10.5 mm. Samples were analysed using Oxford Instruments EDS X-ray analysis. The standards used were a mixture of natural minerals, metal oxides and pure metals, as calibrated by the factory. Oxygen contents were determined by stoichiometry.

Organic carbon and sulfur contents were measured in black shales of the Moffat Shale Group using a LECO CS225 elemental analyser, after decarbonatization with hydrochloric acid, to a precision of ±0.05%.

There are several assessments of how to reconstruct the original carbon content before hydrocarbon generation (e.g. Raiswell and Berner 1987; Pang *et al.* 2014; Allan *et al.* 2016; Daly and Edman 2019). The carbon loss is related to kerogen type, increasing from the relatively recalcitrant kerogen type III to the oil-prone type I. Lower Paleozoic graptolitic shales are considered to have a composition approximating to kerogen type II (Gupta *et al.* 2006;

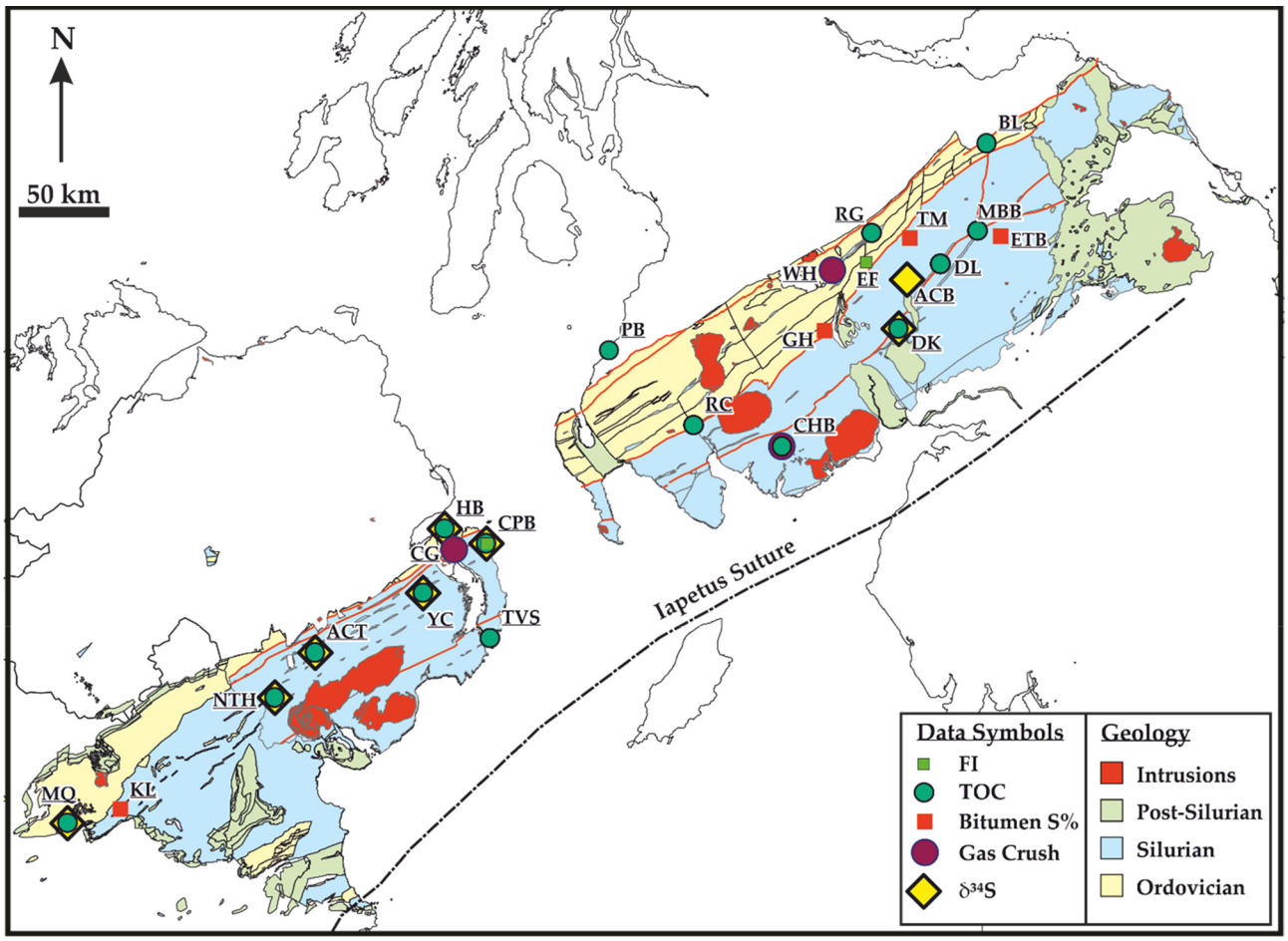

Fig. 1. Map of Southern Uplands-Down-Longford Terrane, showing sample localities for petrographic study and geochemical analysis.

Luo *et al.* 2020). The carbon content of kerogen type II is reduced to about a third to a half of the original content by the time it is through the gas window. We adopt a conservative value of 50% carbon loss. The hydrocarbon source rock potential is evaluated using a plot of TOC and Hydrogen Index (after Çiftçi *et al.* 2010).

Sulfur isotopes

For sulfur isotope analysis, pyrite samples from the Moffat Shale were combusted with excess Cu_2O at 1075°C in order to liberate the SO_2 gas under vacuum conditions. Liberated SO_2 gases were analysed on a VG Isotech SIRA II mass spectrometer, with standard corrections applied to raw $\delta^{66}SO_2$ values to produce true $\delta^{34}S$ values. The standards employed were the international standard NBS-123, IAEA-S-3, and SUERC standard CP-1.

Fluid inclusions

Fluid inclusions were measured in samples from Elvanfoot and Coalpit Bay, where bedding-parallel quartz veining is well developed in black shale, and contains bitumen in the latter case. Fluid inclusion studies were performed on doubly polished wafers using a Linkam THMS-600 heating–freezing stage mounted on a Nikon Labophot transmission light microscope. The instrument equipped with a range of objective lenses including a 100× lens, was calibrated against synthetic H_2O (374.1 and 0.0°C) and CO_2 (−56.6°C) standards (Synthetic Fluid Inclusion Reference Set, Bubbles Inc., USA). Approximate pressure corrections were made following the approach of Goldstein and Reynolds (1994).

Gas analysis

A test of methane generation, which could have been evolved during maturation, was made using quantitative fluid inclusion gas analysis (Blamey 2012). Fluid inclusion volatile analysis was done in vacuum using the CFS (crush-fast scan) method at University of Western Ontario's Fluid Inclusion Gas laboratory. Samples were first cleaned with NaOH to reduce surface organic contamination, and then were rinsed with deionized water. *c.* 0.1 gram of sample was incrementally crushed under a vacuum of *c.* 10^{-8} Torr yielding two to ten crushes per sample. The analyses were performed by means of two Pfeiffer Prisma quadrupole mass spectrometers operating in fast-scan, peak-hopping mode. The system routinely analysed for a range of gases including methane and carbon dioxide. The instrument was calibrated using commercial gas mixtures, synthetic inclusions, and in-house fluid inclusion gas standards. Samples were analysed from five localities; at Helen's Bay, Coalpit Bay and Coalheugh Burn where veins record the chemistry of fluids through black shales during their Lower Paleozoic maturation, and Conlig and Wanlockhead, where veins record post-prism, Upper Paleozoic mineralization history. Data are recorded on a reference cross-plot of carbon dioxide/methane and nitrogen/argon ratios, used to distinguish fluids originating in different environments (Blamey 2012).

Results

Petrography

Migrated bitumen (hydrocarbon residues that clearly post-date deposition) occurs in the SUDLT prism rock as:

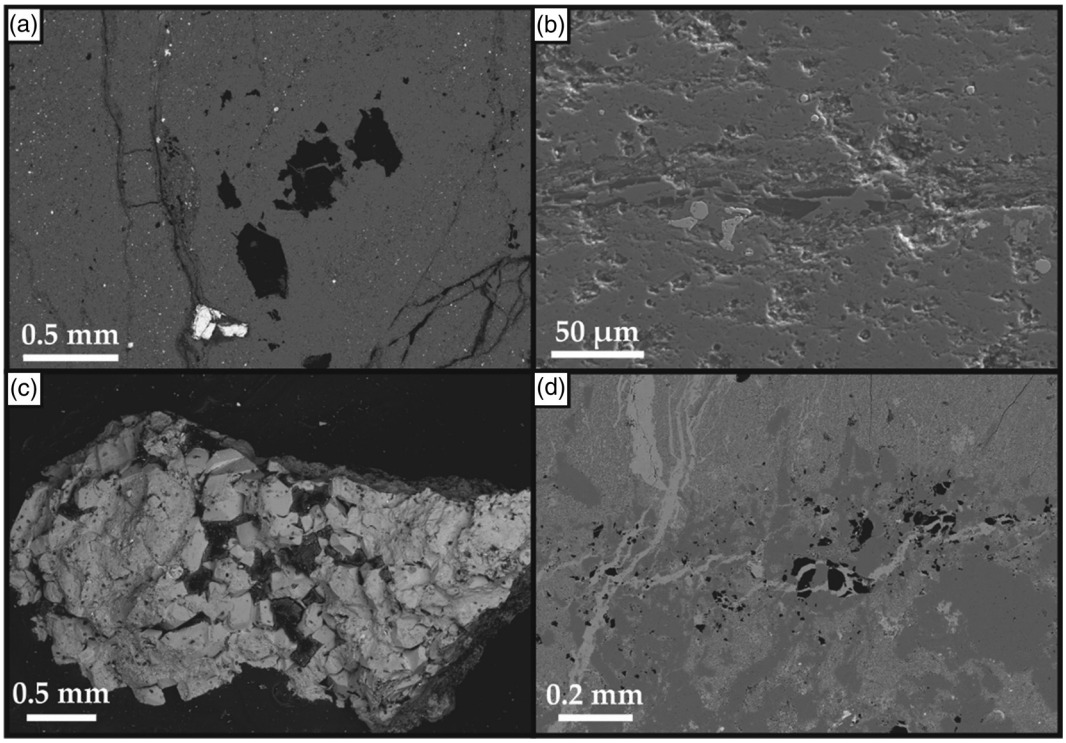

Fig. 2. Electron micrographs of migrated bitumen. (**a**) Bitumen (black) in quartz vein, Molly Quarry, (**b**) Bitumen (dark) in quartz vein (horizontal in image), Newtonhamilton, (**c**) Bitumen (black) in quartz vein, Glengar Hill, (**d**) Bitumen (black) in calcite veinlets cutting through shale, Tweedsmuir.

(i) Small (usually <1 cm) lenses along bedding surfaces in the Moffat Shale (Fig. 2). The surfaces may anastomose, following bedding-parallel deformation.
(ii) Masses larger than above which cross-cut the shales where they are heavily deformed, including near fault structures.
(iii) Traces along fractures through greywackes, usually mineralized by calcite/quartz (Figs 2, 3). Many dark veins cut the greywackes, but they consist of phyllosilicates such as illite and/or chlorite (Needham 2004).

Measurement of 59 Moffat Shale samples from 14 localities in Scotland and Ireland yield organic carbon contents (Table 1) mostly in the range 2 to 5% TOC with a mean value of 2.45% TOC.

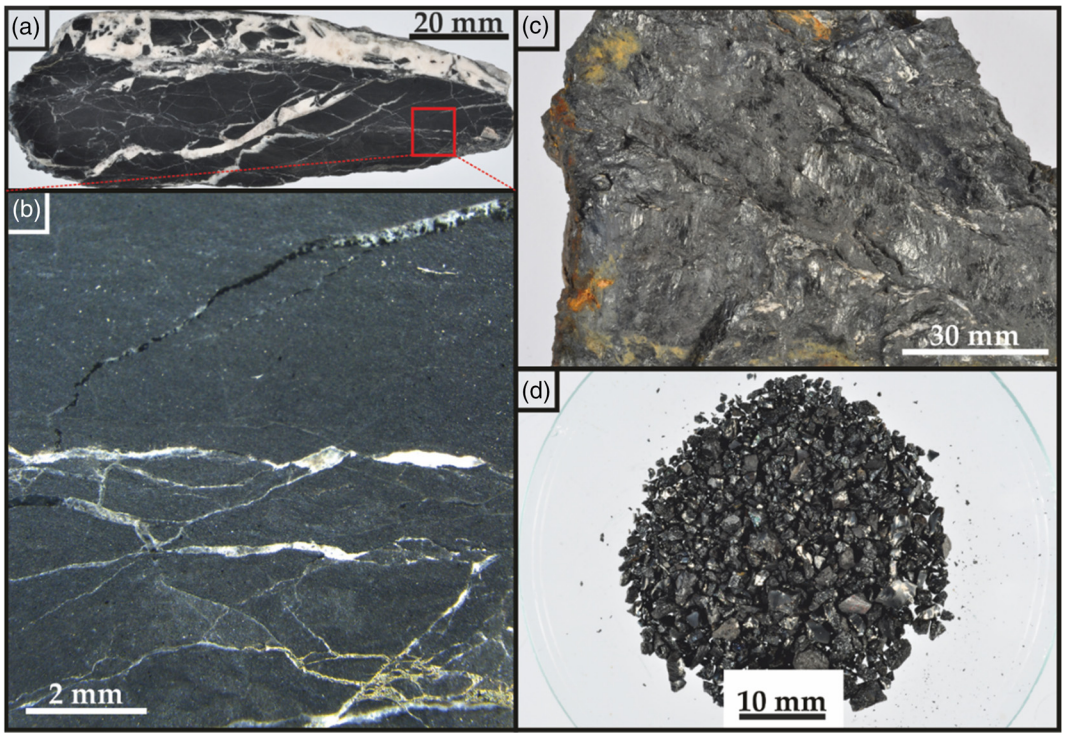

Fig. 3. Specimens from Moffat Shale localities. (**a**) Extensive bedding-parallel veining, Coalpit Bay, (**b**) Close-up of A, showing bitumen (black) and pyrite (golden) within calcite veins, (**c**) Coal-like rock with polished movement surfaces, Lindean, (**d**) Bitumen fragments, Kill Mine, Kilnaleck.

Table 1. *Total Organic Carbon (TOC) and Total Sulfur (TS) contents (%) for black shale samples, Southern Uplands-Down-Longford Terrane*

Locality	Map code	Grid reference	No. anals. (*n*)	Mean TOC (%)	Mean TS (%)
Scotland					
Coalheugh Burn	CHB	NX 680593	5	3.12	0.78
Broad Law	BL	NT 347532	1	1.39	0.22
Dob's Linn	DL	NT 196158	10	2.09	2.21
Duffkinnel	DK	NY 060957	3	1.46	0.03
Mount Benger Burn	MBB	NT 314259	3	3.74	2.41
Pinbain Burn	PB	NX 142916	1	2.81	0.91
Rein Gill	RG	NS 981259	2	2.38	1.21
River Cree	RC	NX 401669	3	0.90	0.16
Ireland					
Coalpit Bay	CPB	J 595788	6	1.26	1.75
Helen's Bay	HB	J 459831	1	1.43	4.60
Yates Corner	YC	J 396623	7	2.87	0.71
Acton	ACT	J 053421	5	1.50	0.83
Newtownhamilton	NTH	H 926273	11	3.87	1.47
Molly Quarry	MQ	N 255855	1	1.63	2.52
Weighted mean			59	2.45	1.36

Previous data for the Moffat Shales are similarly in the range 2–4% TOC (Thickpenny and Leggett 1987). Much other published TOC data for shales, especially for the Dob's Linn section, is at the 1–2% level (Hammarlund *et al.* 2012; Koehler *et al.* 2019; Bond and Grasby 2020). Adopting the value of 50% carbon loss for shales with type II kerogen indicates an original mean content of up to 10%. Measurements of the hydrogen index for graptolitic carbon give values in the range up to 500 mg/g TOC (Bustin *et al.* 1989; Luo *et al.* 2020).

The carbon content range of 2 to 5% TOC, even before reconstruction of the original content of double this value, and an assumed hydrogen index in the range 300 to 500 mg/g TOC for type II kerogen rich in graptolites place the rocks in the excellent/excellent category of an evaluation diagram for hydrocarbon source rocks (Fig. 4).

The post-prism fluids are over 99% water, while the syn-prism fluids contain up to 30% non-aqueous gas (Table 2). The evaluation of methane in syn-prism and post-prism fluids is made by their carbon dioxide/methane ratios, which avoids complexity due to variations in the abundance of fluid inclusions and contributions of other gases. The data from the syn-prism and post-prism samples mostly plot separately, with some minor overlap (Fig. 5). The syn-prism gas data plot particularly in the region of organic-derived fluids, while the post-prism gas data plot in the fields of shallow meteoric and evolved crustal fluids.

The carbon dioxide/methane ratio varies from 0.03 to 1.34 (mean 0.17, $n = 22$) in the syn-prism veinrock at Helen's Bay, Coalpit Bay and Coalheugh Burn and from 0.14 to 26.32 (mean 7.23, $n = 30$) in the post-prism veinrock at Conlig and Wanlockhead. In summary, the syn-prism rocks contain a higher proportion of methane. Few measurements of modern gas seepages are available in the SUDLT, but a single borehole in Ordovician rocks contains a high (150 µg/L) methane level (Bell *et al.* 2016). In addition, the syn-prism veinrock samples contain hydrogen, which is completely absent from the post-prism veinrock. Examples of fluid composition are given in Table 2.

A collation of localities in Ireland and Scotland where attempts to mine 'coal' were made in the Ordovician–Silurian rocks of the SUDLT prism (Fig. 6) includes some places where fuel was actually produced and used. Most of the productive localities were in Ireland,

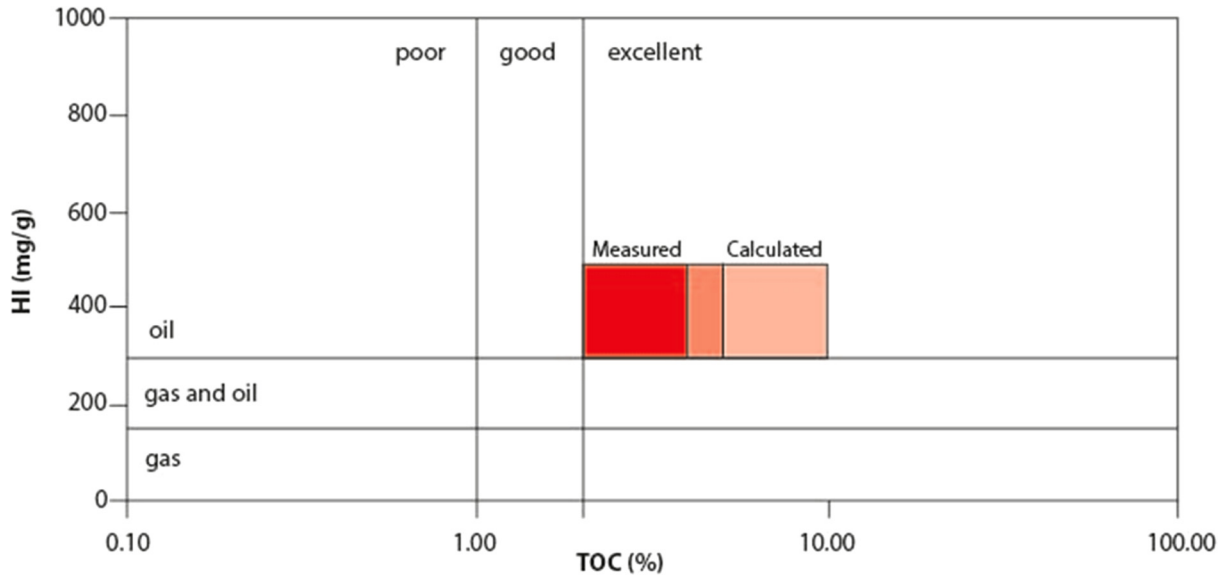

Fig. 4. Cross-plot of ranges of total organic carbon (TOC) content v. inferred Hydrogen Index (HI), indicating that the carbonaceous shales have an excellent capacity to generate oil (template after Çiftçi *et al.* 2010). Original TOC content assumes 50% loss from kerogen type II during maturation. Data sources in text.

Table 2. *Representative cold-crush gas analyses for samples of syn-prism veinrock, and post-prism veinrock*

Locality	Coalpit Bay (syn-prism)	Coalheugh Burn (syn-prism)	Conlig (post-prism)	Wanlockhead (post-prism)
Water (wt%)	89.68	73.90	99.49	99.70
CH_4	9.38	24.25	0.01	0.04
CO_2	0.78	1.33	0.16	0.20
H_2	0.04	0.05	0.00	0.00
He	0.0002	0.0003	0.0002	0.0003
N_2	0.12	0.47	0.34	0.04
Ar	0.0003	0.0006	0.0042	0.0008
H_2S	0.0000	0.0003	-	0.01
CO_2/CH_4	0.08	0.06	15.56	4.47
N_2/Ar	479	834	80	51
Mols gas (non-aqueous)	1.59×10^{-10}	1.58×10^{-09}	1.02×10^{-10}	1.03×10^{-10}

especially the Kilnaleck coal mine (Moore 1872*a*, *b*; McEvoy 1885). The full archive of localities is given in Supplementary Material (Table S1).

Bitumen in the Moffat Shale from several localities has a mean sulfur content which varies from 0.17 to 0.96% (Table 3).

The mean sulfur content in the Moffat Shale is about 1.4% (Table 1), reflecting an abundance of pyrite. Pyrite is mostly finely disseminated, but it also forms megascopic seams (Armstrong and Coe 1997), and there is additionally pyrite in cross-cutting fractures. Pyrite yielded sulfur isotope compositions from 21 samples (Table 4; Fig. 7). The compositions are bimodal, comprising a light range (−17 to −45 ‰) and a heavier range (+3 to −10 ‰). Most samples of pyrite in a detailed profile through the Moffat Shale section at Dob's Linn are also lighter than −20 ‰ (Hammarlund *et al.* 2012).

Bedding-parallel quartz in the Moffat Shale at Coalpit Bay yields a range of primary fluid inclusion homogenization temperatures from 132 to 155°C ($n = 10$) and a salinity of 11–12 wt% equiv. NaCl ($n = 4$). Accounting for a pressure correction at several kilometres depth, the temperature was probably at least 200°C. Bedding-parallel quartz from Elvanfoot yields two populations of primary fluid inclusions. These yield homogenization temperatures of 150–170°C ($n = 27$) and 220–240°C ($n = 21$).

Discussion

Structural context

The pattern of late diagenesis/low-grade metamorphism was acquired during the development of the accretionary architecture, when the strata were already steely dipping, i.e. stacking of thrust slices commenced at lower than final temperatures (Merriman and Roberts 2000). Structural evolution particularly involved movement on the Moffat Shale horizons, repeated by the stacking process. The shale-turbidite boundaries exhibit progressive deformation from soft-sediment movement to anastomosing shear zones containing multiple generations of calcite and quartz veins, with subsidiary phyllosilicates and sulfides (Needham 2004). Fractures in the turbidites similarly show progression from partly lithified faults to mineralized brittle fractures. The veining focused in the shale horizons likely reflects dilatant fracturing following a build-up of high fluid pressure due to low permeability (Needham 2004). The turbidites are composed of greywackes, which have low permeability due to an abundance of matrix clay (MacDonald *et al.* 2007). The extensive quartz and carbonate veining is typical of accretionary prisms, in which precipitation implies large volumes of fluid flow through limited fracture space (Fisher and Byrne 1990; Moore and Vrolijk 1992).

Hydrocarbon generation

The TOC contents measured in the Moffat Shale are much higher than those reported in a worldwide review of subduction zone sediments (Japan, Alaska, Costa Rica, Barbados, Mariana), which are almost all less than 1 wt% TOC (Raimbourg *et al.* 2017). Hydrocarbon generation in an environment of high TOC, and temperature increase faster than normal burial, would be abnormal. A hydrocarbon source rock with exceptional generating capacity (excellent carbon content and hydrogen index) can produce huge

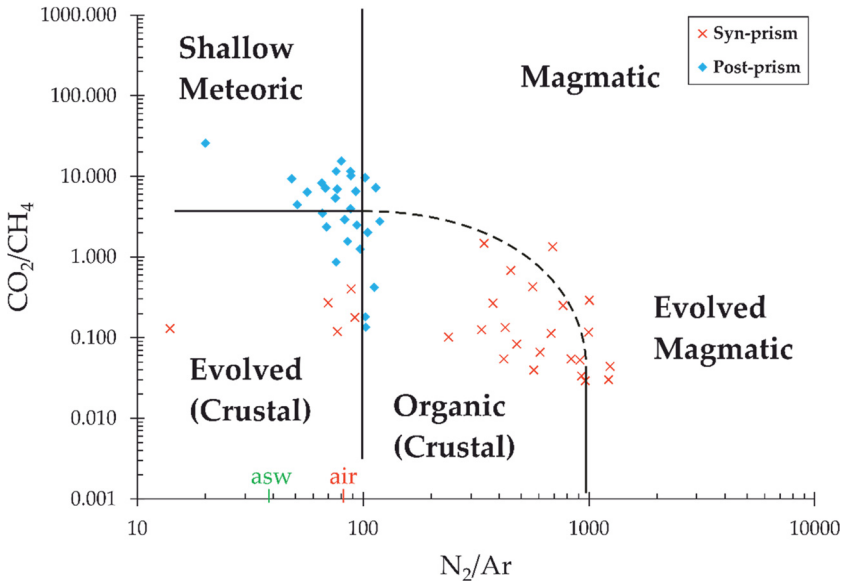

Fig. 5. Cross-plot of carbon dioxide/methane and nitrogen/argon ratios from crush-gas analyses of quartz veins through SUDLT prism rocks and cross-cutting post-prism mineralization (reference template modified from Blamey 2012). Carbon dioxide/methane ratios are much lower, and nitrogen/argon ratios much higher, in syn-prism mineralization.

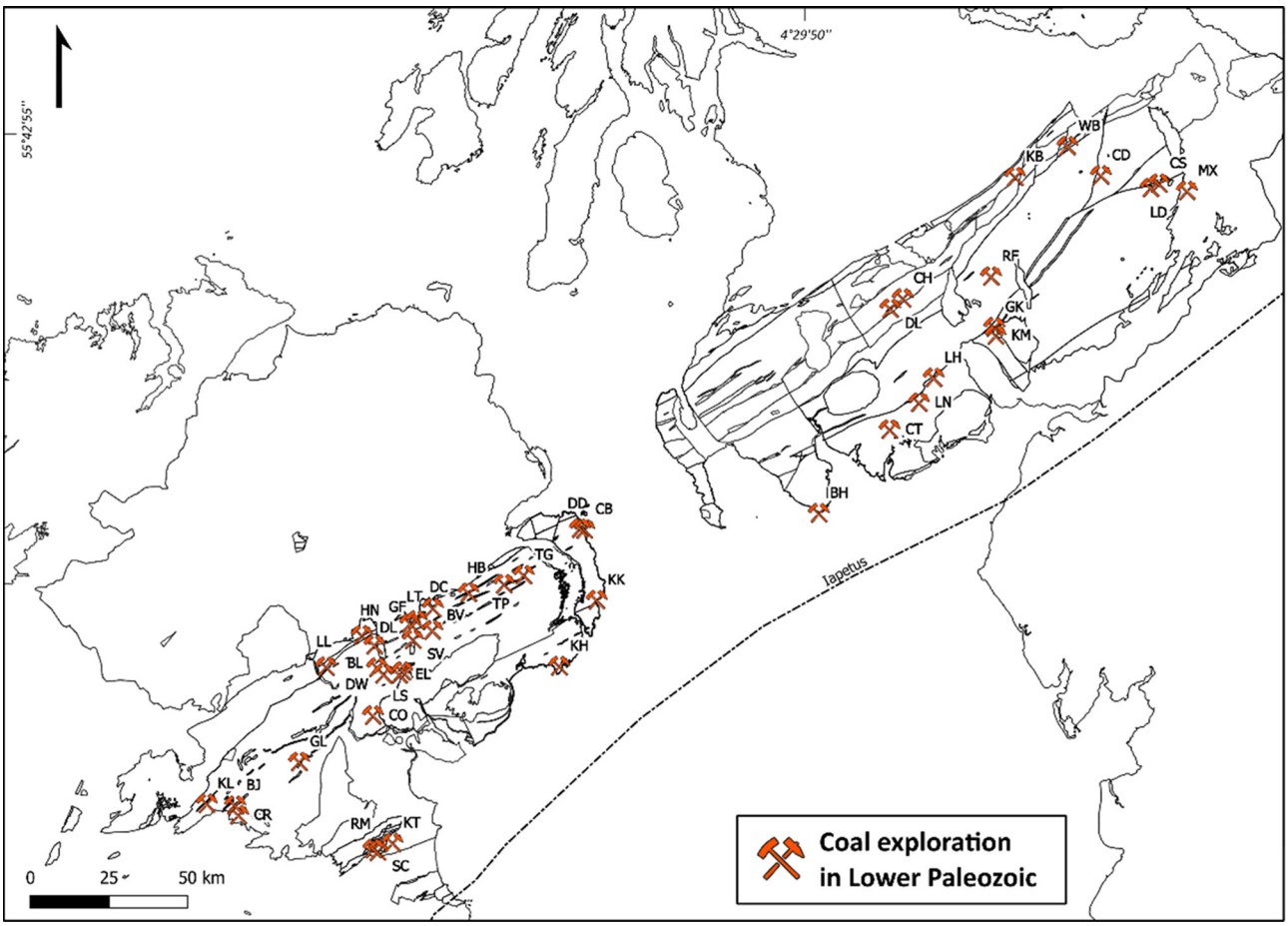

Fig. 6. Map of Southern Uplands-Down-Longford Terrane, showing localities where attempts were made to mine for 'coal'.

volumes of oil once it enters the oil window. This may be achieved by structural repetition in thrust belts including accretionary prisms (Edman and Surdam 1984; Gusterhuber *et al.* 2013; Lyu *et al.* 2020). If the oil window is entered rapidly because of rapid tectonic loading, the result may be a catastrophic addition of fluid that has little space to enter. The sequence of shales and turbiditic greywackes with very low porosity provided negligible opportunities for the migration of hydrocarbons, which would then be under high fluid pressure. The result was the retention of hydrocarbons in rock matrix and pooling of hydrocarbons along bedding surfaces within the source rock, so-called in-source reservoirs with in-source bitumen (Mastalerz *et al.* 2018; Yao *et al.* 2021). The early–formed bitumen could be a significant component of the total hydrocarbons.

As liquid hydrocarbons, and the first-formed bitumen, are progressively buried, including within in-source reservoirs, they are heated to the point where they undergo cracking to yield methane-rich gases and a solid residue (Xiong *et al.* 2016; Raimbourg *et al.* 2017; Zhao *et al.* 2017). Typically, the cracking commences at about 135 to 150°C (Zhao *et al.* 2017; Sanei 2020), or even lower if the hydrocarbons are sulfur-bearing (Kelemen *et al.* 2010; Mastalerz *et al.* 2018), which was reached and exceeded in the SUDLT. The entrained gas in syn-prism veinrock is methane-rich, while the gas in post-prism veinrock is carbon dioxide-rich. The carbon dioxide/methane ratio is over an order of magnitude lower in the syn-prism veinrock. This distinction supports a model of cracking of hydrocarbons to produce the solid bitumen, and the cessation of organic maturation by the time of Upper Paleozoic mineralization.

Cracking of the organic matter to liberate methane would further increase the fluid pressure (Raimbourg *et al.* 2017), while leaving a solid bitumen residue. The generation of hydrocarbons would make detachment on the bedding surface much easier (Cobbold *et al.* 2004; Zanella *et al.* 2014; Pereira *et al.* 2018). This would add to the phyllosilicate growth (Merriman *et al.* 1995) and water-rich bentonites in the Moffat Shale (McCurry and Anderson 1989) which both accommodated bedding-parallel movement.

Table 3. *Sulfur contents of migrated bitumen, Southern Uplands-Down-Longford Terrane*

Locality	Grid Reference	Host rock	No. measurements	Mean sulfur content (%)
Molly Quarry, Co. Longford	N 255855	Quartz in black shale	22	0.72
Newtownhamilton, Co. Armagh	H 925274	Quartz in black shale	7	0.96
Kilnaleck, Co. Cavan	N 430905	'Coal' vein in black shale	10	0.50
Helen's Bay, Co. Down	J 459831	Vein in greywacke	18	0.36
Coalheugh Burn, Dumfries & Galloway	NX 679593	Quartz in black shale	20	0.68
Glengar Hill, Dumfries & Galloway	NX 825957	Vein in greywacke	8	0.17
Ettrickbridge, Scottish Borders	NT 386242	Vein in greywacke	10	0.44
Tweedsmuir, Scottish Borders	NT 101241	Vein in greywacke	11	0.54

Table 4. *Sulfur isotope compositions for pyrite in Southern Uplands-Down-Longford Terrane*

Sample ID	Locality	Grid Reference	$\delta^{34}S_{VCDT}$ (‰)	Notes
ACT1	Acton	J 053421	−23.6	Replaced graptolite
ACT2	Acton	J 053421	−22.7	Replaced graptolite
ACT3	Acton	J 053421	−23.7	Replaced graptolite
CAT28-dS1	Auchencat Burn	NT 090110	−19.8	Cu-Bearing
CAT28-dS2	Auchencat Burn	NT 090110	−19.2	Cu-Bearing
CPB1	Coalpit Bay	J 595788	−25.8	
CPB2	Coalpit Bay	J 595788	−25.8	
CAT18-dS3	Coalpit Bay	J 595788	−44.5	
CAT23-dS1	Duff Kinnel	NY 060957	−29.7	
MQ1	Molly Quarry	N 255855	−19.8	
MQ2	Molly Quarry	N 255855	−18.0	
MQ3	Molly Quarry	N 255855	−18.7	
ST315-dS4	Molly Quarry	N 255855	−16.8	
YC1	Yates Corner	J 396623	−27.2	
YC2	Yates Corner	J 396623	−28.3	
JGA 355	Newtonhamilton	H 926273	−2.0	Bedding Parallel; Euhedral
ST355-dS2	Newtonhamilton	H 926273	−1.0	Bedding Parallel; Euhedral
ST355-dS4	Newtonhamilton	H 926273	−10.3	Oblique Vein
HB1	Helen's Bay	J 459831	2.2	Euhedral
HB2	Helen's Bay	J 459831	2.4	Euhedral
HB3	Helen's Bay	J 459831	2.2	Euhedral

The occurrence of hydrogen with methane in the syn-prism veinrock is probably also a product of thermal maturation. The two gases are released together during pyrolysis of carbonaceous shales, which simulates thermal maturation (Li *et al.* 2015). Thermally mature organic matter can be made to release hydrogen in an industrial process using catalysts and it is speculated that this would occur naturally on a geological timescale (Huang *et al.* 2021). The most thermally altered coals also yield hydrogen (Zgonnik 2020). Suzuki *et al.* (2017) showed that carbonaceous shales in the temperature range up to 200°C would yield methane, then progressively start generating hydrogen instead.

The composition of typical fluids from recent and ancient accretionary prisms is evident from cold seeps. The fluids in cold seeps and hydrothermal vents on the sea floor are dominated by methane and hydrogen sulfide, but also include molecular hydrogen (Newell *et al.* 2007; Dong *et al.* 2020). The fluids trapped within the SUDLT are thus consistent with the fluids that emerge as seeps.

The high nitrogen/argon ratios in the syn-prism fluids reflect liberation of nitrogen from organic matter during thermal maturation (Gai *et al.* 2020). Lower Paleozoic black shales, including Ordovician shales at Dob's Linn in the SUDLT, are nitrogen-bearing (Kiipli and Kiipli 2013; Gai *et al.* 2020), and as nitrogen content increases with the content of organic matter (Kiipli and Kiipli 2013), highly carbonaceous shales can yield more nitrogen.

The temperature range inferred from fluid inclusions in bedding-parallel veins at Coalpit Bay and Elvanfoot (cooler population) is

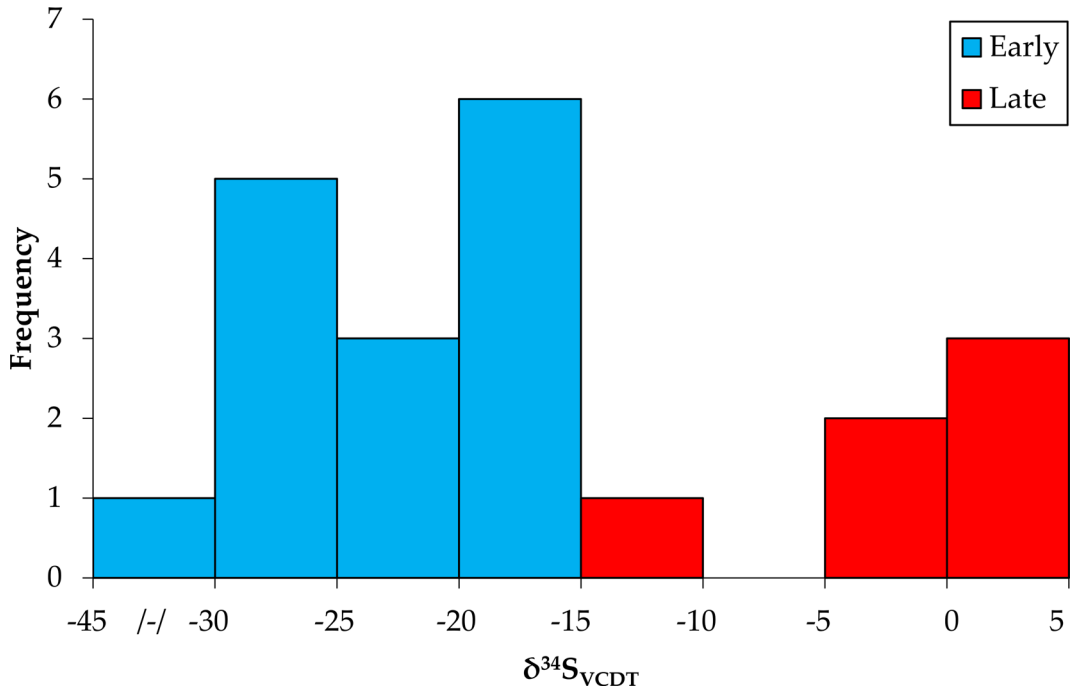

Fig. 7. Sulfur isotope data (‰ CDT) for pyrite in Moffat Shale, Scotland, Northern Ireland and Republic of Ireland. Values for early pyrite are lighter than −15 ‰, which reflects microbial sulfate reduction during diagenesis. A smaller population of near-zero values were obtained from late, vein-hosted pyrite.

comparable to the temperatures of 150–320°C inferred from chlorite compositions (Merriman *et al.* 1995) and 170–300°C from Raman spectroscopy of organic carbon (Schito *et al.* 2022) in the SUDLT prism (Fig. 8). This is also the temperature range of maximum release of hydrous fluids in accretionary prisms (Massonne and Willner 2008; Willner *et al.* 2009), and the cracking of organic matter within prisms (Raimbourg *et al.* 2017). Bedding plane slip and decollement are typically initiated at temperatures of 100–200°C (Raimbourg *et al.* 2017), which is consistent with thrust stacking at lower than final temperature in the SUDLT.

Elsewhere in the SUDLT in two base metal-bearing deposits in County Down, two populations of fluid inclusions have been identified in quartz veins (Baron and Parnell 2005). A population with temperatures 220 to 360°C is followed by a set with temperatures 70 to 240°C, attributed to heating by Caledonian intrusions and Carboniferous–younger base metal mineralization, respectively. Both populations are probably younger than the inclusions in black shales, although the higher set of temperatures at Elvanfoot may represent the Caledonian heating. Caledonian plutons in the Southern Uplands are Devonian age, so post-dated the deformation during accretion, and may have been emplaced using the existing shear fabric of the prism (Brown *et al.* 2008).

The cracking process leaves a high proportion, up to 50%, of the original oil as a solid (Xiong *et al.* 2016; Zhao *et al.* 2017). Thus, in the SUDLT where very rich source rocks yielded substantial amounts of oil that could not migrate, large deposits of solid bitumen could be formed. This history of hydrocarbon generation explains the formation of the bitumen mined as ‘coal’ in several parts of the SUDLT (Fig. 6).

In addition to cracking of kerogen to produce bitumen, it is possible that bitumen was cracked to produce more thermally altered bitumen (pyrobitumen) and gas. This is a process which contributes to the formation of gas, including shale gas, at temperatures above 150°C (Uguna *et al.* 2016; Meredith *et al.* 2019). Large amounts of pyrobitumen occur in some gas reservoirs (e.g. Wang *et al.* 2021; Li *et al.* 2022). Where bitumen is cut by calcite or quartz in the SUDLT (Fig. 2), we have not observed a second phase of bitumen formation in the veins. However, additional maturation may not have produced a new solid, but just altered the existing solid and generated gas.

The temperatures indicated by Raman Spectroscopy, from 200 to 300°C (Schito *et al.* 2022), indicate the maximum temperature reached, which were probably higher than the temperature of bitumen formation in many cases. However, bitumen at Clontibret, Ireland (Schito *et al.* 2022), which is associated with antimony mineralization (Fig. 9) at about 300°C (Steed and Morris 1986) implies that at least some bitumen was deposited at a temperature high enough to suggest that cracking of a previous solid was possible.

Sulfur isotopes

Further insight stems from the sulfur isotope composition of pyrite in the black shale. The pyrite can be divided into precipitates from two stages:

(i) Finely disseminated pyrite, which forms framboids visible using electron microscopy (Fig. 10); together with pyrite

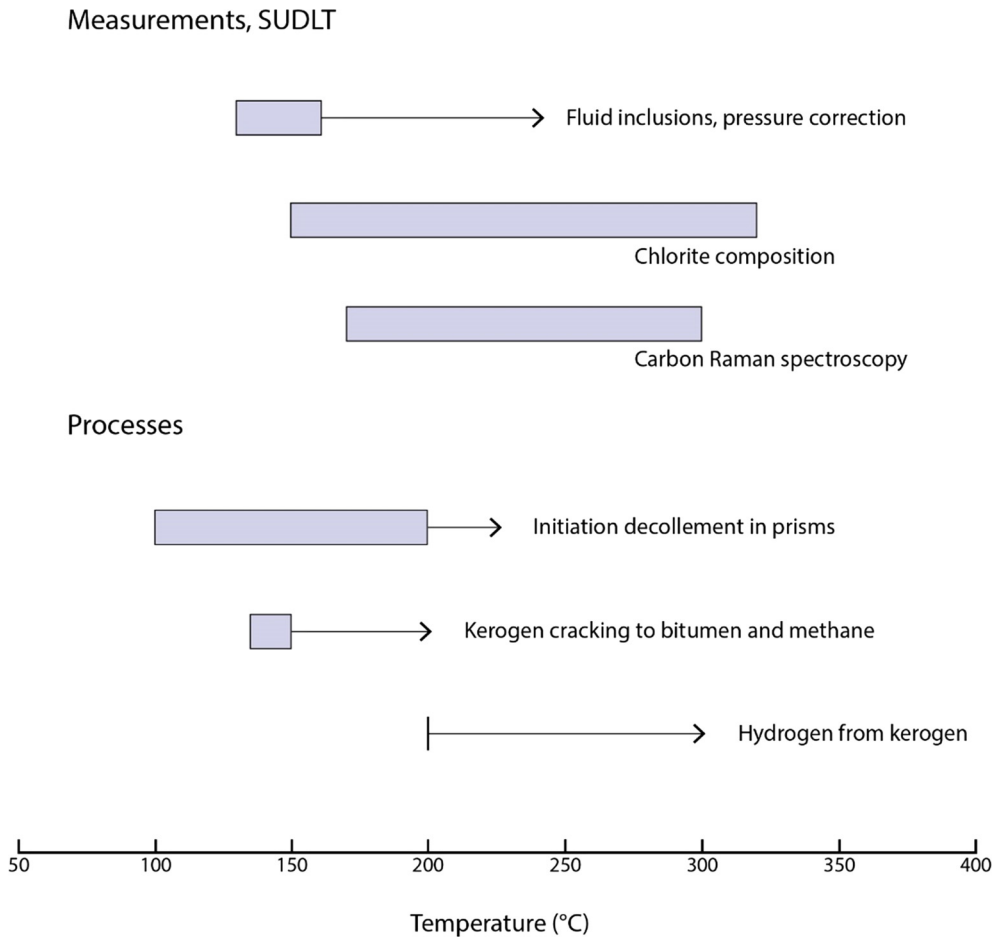

Fig. 8. Temperatures inferred from measurements of SUDLT rocks (fluid inclusion homogenization temperatures, chlorite compositions, Raman spectroscopy of carbon), and processes in accretionary prism shales (decollement, cracking of kerogen, hydrogen generation). Data sources in text.

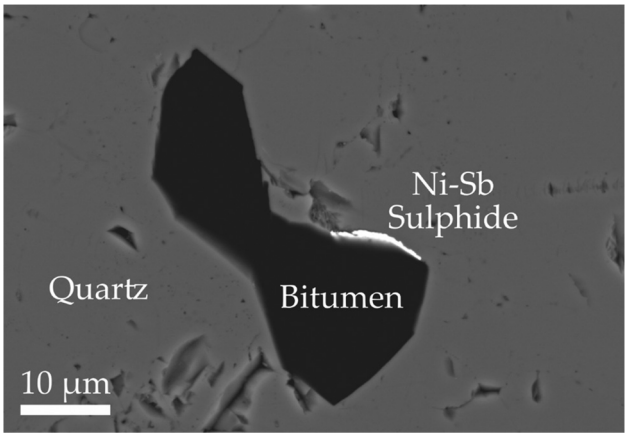

Fig. 9. Bitumen in quartz vein, Clontibret, SUDLT (close to BL on Fig. 6), with associated antimony (Sb) mineralization (bright) formed at about 300°C.

which replaces graptolite fossils. These occurrences are attributed to (early) diagenesis, before any deformation.

(ii) Pyrite crystals up to 2 mm size, which occur along brittle fractures, either parallel to bedding planes or oblique to them. The fractures also carry bitumen and quartz. The fractures are post-compaction, and they must be related to deformation.

The two stages of pyrite are matched by the bimodal distribution of sulfur isotope compositions. The diagenetic pyrite has a light isotope composition (mean −24.2 ‰), while the vein-filling pyrite has a heavier composition (mean −1.1 ‰). The light values are typical of pyrite precipitated by microbial sulfate reduction (MSR) at low temperatures (Machel 2001). The heavier composition is sufficiently different that it is very unlikely to be simply derived from the light pyrite, which implies that a new supply of sulfur was introduced. Three explanations that may have contributed to this heavier composition are closed system modification of existing sulfur (e.g. Bonnetti *et al.* 2020), introduction of magmatic sulfur from igneous rocks, and thermochemical sulfate reduction (TSR). Limited evidence from pyrite in Ordovician basalts in the region (excepting vesicular pyrite derived by microbial sulfate reduction of sea water) indicates it has a zero to positive signature (Parnell *et al.* 2015), so this composition would have been available for possible release at elevated temperature. Thermochemical sulfate reduction is commonly associated with bituminous residues, especially bitumen enriched in sulfur (Machel 2001; Kelemen *et al.* 2010; Walters *et al.* 2015). The measured sulfur content in the prism bitumen could be an indicator of TSR, but the contents are not high. The bitumen and quartz within the same fractures imply a temperature range >100°C, when TSR and associated cracking of oil to solid bitumen could occur (Kelemen *et al.* 2010; Mastalerz *et al.* 2018). However, TSR would not yield such light isotopic compositions from seawater with a composition of almost 30 ‰ (Machel 2001; Hu *et al.* 2021). Closed system behaviour would be consistent with the overpressure typical of an accretionary prism. The heavier $\delta^{34}S$ signature of the second stage pyrite would reflect more complete sulfate reduction associated with a strong enrichment of residual ^{34}S, during the transition from an open to a closed system. Data from a modern accretionary setting indicate that this is a feasible explanation. Bottrell *et al.* (2000) reported pyrite compositions from the Cascadia Margin accretionary wedge which transition from shallow light values due to MSR to deeper much heavier values when oxidation of the shallow pyrite had liberated new sulfate for further reduction.

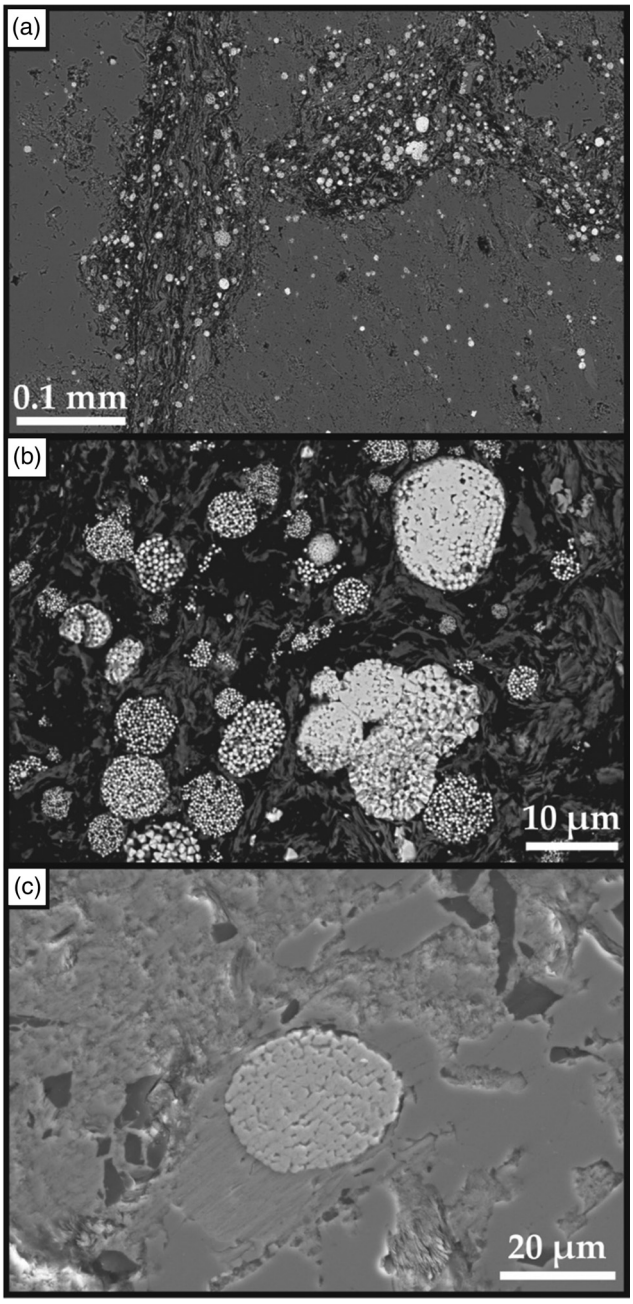

Fig. 10. Electron micrographs of pyrite framboids, Southern Uplands. (**a**) Framboids in bitumen-rich shale, Coalheugh Burn, (**b**) Close-up of A, showing framboids in matrix of bitumen (black), Coalheugh Burn, (**c**) Framboid and bitumen (black), calcite veining, Tweedsmuir.

The SUDLT is cross-cut by base metal sulfide mineralization, formerly mined, including at Leadhills-Wanlockhead, Scotland and Conlig, Ireland (Rice *et al.* 2018), and at the western end is overlain by the giant zinc deposit in Carboniferous rocks at Navan. These ore deposits were formed in the Upper Paleozoic, after prism evolution was complete, but it is likely that some of the sulfur in the deposits was derived from the sulfur-rich prism rocks which they cross-cut (Rice *et al.* 2018). The SUDLT contains stratabound metal anomalies located in carbonaceous shales, including a copper-rich black shale belt near Moffat (British Geological Survey 1993). The black shales have also been implicated as a host to gold mineralization during Caledonian deformation, and the carbon suggested as a ligand to promote gold transport (Naden and Caulfield 1989; Rice *et al.* 2018). Thus, both Caledonian and post-Caledonian mineralization may be a legacy of the organic-rich oceanic sediments which sequestered abundant diagenetic pyrite.

The Lower Paleozoic

The high hydrocarbon yield and association with sulfides ultimately reflects the nature of Ordovician oceanic sedimentation, which was characterized by anoxia, especially during the late Ordovician-early Silurian (Berry 2010; Landing 2011; Bartlett *et al.* 2018; Edwards *et al.* 2018; Stockey *et al.* 2020). The anoxic environment allowed both high burial of organic matter, and associated sulfide precipitation during early diagenesis. The sulfidic nature of the anoxia, which is implicated in the Late Ordovician mass extinction, is documented specifically in the SUDLT (Hammarlund *et al.* 2012; Dahl *et al.* 2021).

The abundance of sulfides precipitated due to the high organic carbon content in the seafloor sediments potentially also sequestered a large quantity of trace elements including base metals (Gregory *et al.* 2015). Other metals like vanadium and uranium may be concentrated directly by the reductive properties of the organic matter (Parnell 2022). Consequently, the carbonaceous nature of the Lower Paleozoic sediments resulted in metal concentrations at the mineable scale elsewhere (e.g. Goodfellow 1987; Bian *et al.* 2021; Parnell 2022). In the SUDLT, syn-prism mineralization was limited to the copper-rich black shales noted above. Cross-cutting gold-antimony mineralization was more likely related to late Caledonian (Devonian) shear zones, which may nevertheless be focused within the black shales (Rice *et al.* 2018).

Several other reports of cracking to yield methane and solid residues are based on Lower Paleozoic successions elsewhere (e.g. Huc *et al.* 2000; Schwangler *et al.* 2000; Zhao *et al.* 2017). This may partly reflect the lower likelihood of younger successions reaching the burial depths and hence temperatures required for cracking to occur. However, the high incidence of cracking in the Lower Paleozoic can be related to the abundance of successions with rich hydrocarbon source rocks due to the anoxia noted above.

The Ordovician–Silurian of NW Europe has been considered a potential resource of shale gas (Schovsbo *et al.* 2012, 2014), especially in the region from Denmark to the Baltic countries. The rocks in Scotland do not contribute to this resource, because of relatively high thermal maturity, and the lack of evidence for any surviving gas volumes.

Conclusions

The Southern Uplands-Down-Longford Terrane accretionary prism is exceptional in including deposits of solid bitumen, which historically have been mined. The bitumen was formed by a singular combination of factors:

(i) The Ordovician oceans were anoxic and buried sediment with carbon contents much higher than in modern subduction zones.
(ii) Rapid maturation due to structural repetition caused generation of large volumes of hydrocarbons.
(iii) The low permeability of shale and intervening turbidite greywackes resulted in high fluid pressure and dilatant fracturing.
(iv) Cracking of the hydrocarbons left solid bitumen within the source rock shales. Additionally, early solid bitumen retained within the rock could have cracked to yield gas and thermally more mature bitumen (pyrobitumen).
(v) Further thermal maturation led to fluids that were anomalously rich in methane, nitrogen and hydrogen.

In addition, the carbonaceous sediment contains abundant pyrite sulfur precipitated by MSR, which contributed sulfur to the hydrocarbons and fracture-hosted sulfides.

Acknowledgements Fluid inclusions were measured by M. Baron. Electron Microscopy was performed with the help of J. Still in the ACEMAC Facility at the University of Aberdeen.

Skilled technical support was also provided by J. Johnston & C. Taylor. P. Carey and A. Lings assisted field sampling. The manuscript benefitted from careful reviews by I. Scotchman and W. Meredith.

Author contributions **JP**: conceptualization (lead), funding acquisition (lead), investigation (equal), methodology (equal), project administration (lead), writing – original draft (lead), writing – review & editing (lead); **JA**: formal analysis (equal), investigation (equal), writing – original draft (supporting); **NJFB**: investigation (supporting), methodology (supporting); **AJB**: investigation (supporting), methodology (supporting); **AS**: investigation (supporting), methodology (supporting); **DM**: investigation (supporting), methodology (supporting), supervision (equal)

Funding This work was funded by the Natural Environment Research Council (NE/T003677/1).

Competing interests The authors declare that they have no known competing financial interests or personal relationships that could have appeared to influence the work reported in this paper.

Data availability All data generated or analysed during this study are included in this published article (and if present, its supplementary information files).

References

Agapitov, I. 2014. Graptolite shale – worldwide distributed Ordovician and Silurian source rock. Paper presented at the SPE Annual Technical Conference and Exhibition, October 2014, Amsterdam, The Netherlands, https://doi.org/10.2118/173477-STU

Allan, A.M., Clark, A.C., Vanorio, T., Kanitpanyacharoen, W. and Wenk, H.-R. 2016. On the evolution of the elastic properties of organic-rich shale upon pyrolysis-induced thermal maturation. *Geophysics*, **81**, D263–D281, https://doi.org/10.1190/geo2015-0514.1

Armstrong, H.A. and Coe, A.L. 1997. Deep-sea sediments record the geophysiology of the late Ordovician glaciation. *Journal of the Geological Society*, **154**, 929–934, https://doi.org/10.1144/gsjgs.154.6.0929

Baron, M.H. and Parnell, J. 2005. Fluid evolution in base-metal sulphide mineral deposits in the metamorphic basement rocks of southwest Scotland and Northern Ireland. *Geological Magazine*, **40**, 3–21, https://doi.org/10.1002/gj.973

Bartlett, R., Elricka, M., Wheeley, J.R., Polyak, V., Desrochers, A. and Asmeron, Y. 2018. Abrupt global-ocean anoxia during the Late Ordovician–early Silurian detected using uranium isotopes of marine carbonates. *Proceedings of the National Academy of Sciences*, **115**, 5896–5901, https://doi.org/10.1073/pnas.1802438115

Beamish, D., Kimbell, G.S., Stone, P. and Anderson, T.B. 2010. Regional conductivity data used to reassess Early Palaeozoic structure in the Northern Ireland sector of the Southern Uplands–Down–Longford terrane. *Journal of the Geological Society*, **167**, 649–657, https://doi.org/10.1144/0016-76492009-122

Bell, R.A., Darling, W.G., Manamsa, K. and Dochartaigh, B.É.Ó. 2016. *The Baseline Concentrations of Methane in Great British Groundwater - The National Methane Baseline Survey*. British Geological Survey Open Report **OR/15/071**.

Berry, W.B.N. 2010. Black shales: an Ordovician perspective. *Special Paper of the Geological Society of America*, **466**, 141–147, https://doi.org/10.1130/2010.2466(09)

Bian, L., Schovsbo, N.H. *et al.* 2021. Molybdenum-uranium-vanadium geochemistry in the Lower Paleozoic Alum Shale of Scandinavia: implications for vanadium exploration. *International Journal of Coal Geology*, **239**, 103730, https://doi.org/10.1016/j.coal.2021.103730

Blamey, N.J.F. 2012. Composition and evolution of crustal, geothermal and hydrothermal fluids interpreted using quantitative fluid inclusion gas analysis. *Journal of Geochemical Exploration*, **116–117**, 17–27, https://doi.org/10.1016/j.gexplo.2012.03.001

Bond, D.P.G. and Grasby, S.E. 2020. Late Ordovician mass extinction caused by volcanism, warming, and anoxia, not cooling and glaciation. *Geology*, **48**, 777–781, https://doi.org/10.1130/G47377.1

Bonnetti, C., Zhou, L., Riegler, T., Brugger, J. and Fairclough, M. 2020. Large S isotope and trace element fractionations in pyrite of uranium roll front systems result from internally-driven biogeochemical cycle. *Geochimica et Cosmochimica Acta*, **282**, 113–132, https://doi.org/10.1016/j.gca.2020.05.019

Bottrell, S.H., Parkes, R.J., Cragg, B.A. and Raiswell, R. 2000. Isotopic evidence for anoxic pyrite oxidation and stimulation of bacterial sulphate reduction in marine sediments. *Journal of the Geological Society, London*, **157**, 711–714, https://doi.org/10.1144/jgs.157.4.711

British Geological Survey 1993. *Regional Geochemistry of Southern Scotland and Part of Northern England*. British Geological Survey, Keyworth, Nottingham.

Brown, P.E., Ryan, P.D., Soper, N.J. and Woodcock, N.H. 2008. The Newer Granite problem revisited: a transtensional origin for the Early Devonian Trans-Suture Suite. *Geological Magazine*, **145**, 235–256, https://doi.org/10.1017/S0016756807004219

Bustin, R., Link, C. and Goodarzi, F. 1989. Optical properties and chemistry of graptolite periderm following laboratory simulated maturation. *Organic Geochemistry*, **14**, 355–364, https://doi.org/10.1016/0146-6380(89)90001-6

Çiftçi, N.B., Temel, R.Ö. and Iztan, Y.H. 2010. Hydrocarbon occurrences in the western Anatolian (Aegean) grabens, Turkey: is there a working petroleum system? *AAPG Bulletin*, **94**, 1827–1857, https://doi.org/10.1306/06301009172

Cobbold, P.R., Mourguesa, R. and Boyd, K. 2004. Mechanism of thin-skinned detachment in the Amazon Fan: assessing the importance of fluid overpressure and hydrocarbon generation. *Marine and Petroleum Geology*, **21**, 1013–1025, https://doi.org/10.1016/j.marpetgeo.2004.05.003

Commission of Inquiry into the Resources and Industries of Ireland 1921. *Memoir on the Coalfields of Ireland*, 2 vols. Dublin.

Dahl, T.W., Hammarlund, E.U., Rasmussen, C.M.R., Bond, D.P.G. and Canfield, D.E. 2021. Sulfidic anoxia in the oceans during the Late Ordovician mass extinctions – insights from molybdenum and uranium isotopic global redox proxies. *Earth-Science Reviews*, **220**, 103748, https://doi.org/10.1016/j.earscirev.2021.103748

Daly, A.R. and Edman, J.D. 2019. Loss of organic carbon from source rocks during thermal maturation. *AAPG Search and Discovery Article*, **60055**, 1–14, https://doi.org/10.1306/60055Daly2019

Dong, X., Rattray, J.E. *et al.* 2020. Thermogenic hydrocarbon biodegradation by diverse depth-stratified microbial populations at a Scotian Basin cold seep. *Nature Communications*, **11**, 5825, https://doi.org/10.1038/s41467-020-19648-2

Edman, J.D. and Surdam, R.C. 1984. Influence of overthrusting on maturation of hydrocarbon in Phosphoria Formation, Wyoming-Idaho-Utah overthrust belt. *AAPG Bulletin*, **68**, 1803–1817.

Edwards, C.T., Fike, D.A., Saltzman, M.R., Lu, W. and Lu, Z. 2018. Evidence for local and global redox conditions at an Early Ordovician (Tremadocian) mass extinction. *Earth and Planetary Science Letters*, **481**, 125–135, https://doi.org/10.1016/j.epsl.2017.10.002

Fisher, D. and Byrne, T. 1990. The character and distribution of mineralized fractures in the Kodiak Formation, Alaska: implications for fluid flow in an underthrust sequence. *Journal of Geophysical Research*, **95**, 9069–9080, https://doi.org/10.1029/JB095iB06p09069

Floyd, J.D. 1996. Lithostratigraphy of the Ordovician rocks in the Southern Uplands: Crawford Group, Moffat Shale Group, Leadhills Supergroup. *Transactions of the Royal Society of Edinburgh: Earth Sciences*, **86**, 153–165, https://doi.org/10.1017/S0263593300002200

Floyd, J.D. 2001. The Southern Uplands Terrane: a stratigraphical review. *Transactions of the Royal Society of Edinburgh: Earth Sciences*, **91**, 349–362, https://doi.org/10.1017/S0263593300008233

Gai, H., Tian, H., Cheng, P., He, C., Wu, Z., Ji, S. and Xiao, X. 2020. Characteristics of molecular nitrogen generation from overmature black shales in South China: preliminary implications from pyrolysis experiments. *Marine and Petroleum Geology*, **120**, 104527, https://doi.org/10.1016/j.marpetgeo.2020.104527

Goldstein, R.H. and Reynolds, T.J. 1994. *Systematics of Fluid Inclusions in Diagenetic Minerals*. *SEPM Short Course*, **31**, Tulsa.

Goodfellow, W.D. 1987. Anoxic stratified oceans as a source of sulphur in sediment-hosted stratiform Zn-Pb deposits (Selwyn Basin, Yukon, Canada). *Chemical Geology*, **65**, 359–382.

Gregory, D.D., Large, R.R. *et al.* 2015. Trace element content of sedimentary pyrite in black shales. *Economic Geology*, **110**, 1389–1410, https://doi.org/10.2113/econgeo.110.6.1389

Gupta, N.S., Briggs, D.E.G. and Pancost, R.D. 2006. Molecular taphonomy of graptolites. *Journal of the Geological Society*, **163**, 897–900, https://doi.org/10.1144/0016-76492006-070

Gusterhuber, J., Hinsch, R., Linzer, H. and Sachsenhofer, R.F. 2013. Hydrocarbon generation and migration from sub-thrust source rocks to foreland reservoirs: the Austrian Molasse Basin. *Austrian Journal of Earth Sciences*, **106**, 115–136.

Hammarlund, E.U., Dahl, T.W. *et al.* 2012. A sulfidic driver for the end-Ordovician mass extinction. *Earth and Planetary Science Letters*, **331–332**, 128–139, https://doi.org/10.1016/j.epsl.2012.02.024

Hu, Y., Cai, C. *et al.* 2021. Distinguishing microbial from thermochemical sulfate reduction from the upper Ediacaran in South China. *Chemical Geology*, **583**, 120482, https://doi.org/10.1016/j.chemgeo.2021.120482

Huang, X., Jin, Z., Liu, Q., Meng, Q., Zhu, D., Liu, J. and Liu, J. 2021. Catalytic hydrogenation of post-mature hydrocarbon source rocks under deep derived fluids: an example of Early Cambrian Yurtus Formation, Tarim Basin, NW China. *Frontiers in Earth Science*, **9**, 626111, https://doi.org/10.3389/feart.2021.626111

Huc, A.-Y., Nederlof, P. *et al.* 2000. Pyrobitumen occurrence and formation in a Cambro–Ordovician sandstone reservoir, Fahud Salt Basin, North Oman. *Chemical Geology*, **168**, 99–112, https://doi.org/10.1016/S0009-2541(00)00190-X

Kelemen, S.R., Walters, C.C. *et al.* 2010. Characterization of solid bitumens originating from thermal chemical alteration and thermo-chemical sulfate reduction. *Geochimica et Cosmochimica Acta*, **74**, 5305–5332, https://doi.org/10.1016/j.gca.2010.06.013

Kiipli, E. and Kiipli, T. 2013. Nitrogen isotopes in kukersite and black shale implying Ordovician-Silurian seawater redox conditions. *Oil Shale*, **30**, 60–17, https://doi.org/10.3176/oil.2013.1.06

Koehler, M.C., Stüeken, E.E., Hillier, S. and Prave, A.R. 2019. Limitation of fixed nitrogen and deepening of the carbonate-compensation depth through the Hirnantian at Dob's Linn, Scotland. *Palaeogeography, Palaeoclimatology, Palaeoecology*, **534**, 109321, https://doi.org/10.1016/j.palaeo.2019.109321

Landing, E. 2011. Time-specific black mudstones and global hyperwarming on the Cambrian-Ordovician slope and shelf of the Laurentia palaeocontinent. *Palaeogeography, Palaeoclimatology, Palaeoecology*, **367–368**, 256–272, https://doi.org/10.1016/j.palaeo.2011.09.005

Leggett, J.K. 1980. British Lower Palaeozoic black shales and their palaeooceanographic significance. *Journal of the Geological Society of London*, **137**, 139–156, https://doi.org/10.1144/gsjgs.137.2.0139

Li, X., Krooss, B.M., Weniger, P. and Littke, R. 2015. Liberation of molecular hydrogen (H2) and methane (CH4) during non-isothermal pyrolysis of shales and coals: systematics and quantification. *International Journal of Coal Geology*, **137**, 152–164, https://doi.org/10.1016/j.coal.2014.11.011

Li, Y., Chen, S.J. *et al.* 2022. Study on the logging response characteristics and the quantitative identification method of solid bitumen at different thermal evolution stages. *Fuel*, **316**, 123424, https://doi.org/10.1016/j.fuel.2022.123424

Luo, Q., Fariborz, G. *et al.* 2020. Graptolites as fossil geo-thermometers and source material of hydrocarbons: an overview of four decades of progress. *Earth-Science Reviews*, **200**, 103000, https://doi.org/10.1016/j.earscirev.2019.103000

Lyu, C., Wang, X. *et al.* 2020. Evaluation of hydrocarbon generation using structural and thermal modeling in the thrust belt of Kuqa Foreland Basin, NW China. *Geofluids*, **2020**, 8894030, https://doi.org/10.1155/2020/8894030

Macdonald, A.M., Ó Dochartaigh, B.E., Kinniburgh, D.G. and Darling, W.G. 2007. *Baseline Scotland: Groundwater Chemistry of Southern Scotland*. British Geological Survey Open Report **OR/08/62**.

Machel, H.G. 2001. Bacterial and thermochemical sulfate reduction in diagenetic settings – old and new insights. *Sedimentary Geology*, **140**, 143–175, https://doi.org/10.1016/S0037-0738(00)00176-7

Makled, W.A., Farouk, S., Al-Hadidy, A.H., Mohammed, I.Q. and Lawa, F.A.A. 2021. Organic petrography of Ordovician – Silurian rocks and their implications to hydrocarbon generation in the Akkas-1 well, western Iraq: new evidence for the Ordovician Gloeocapsomorpha and glaciation events. *Marine and Petroleum Geology*, **128**, 105053, https://doi.org/10.1016/j.marpetgeo.2021.105053

Massonne, H.-J. and Willner, A.P. 2008. Phase relations and dehydration behaviour of psammopelite and mid-ocean ridge basalt at very-low-grade to low-grade metamorphic conditions. *European Journal of Mineralogy*, **20**, 867–879, https://doi.org/10.1127/0935-1221/2008/0020-1871

Mastalerz, M., Drobniak, A. and Stankiewicz, A.B. 2018. Origin, properties, and implications of solid bitumen in source-rock reservoirs: a review. *International Journal of Coal Geology*, **195**, 14–36, https://doi.org/10.1016/j.coal.2018.05.013

McCurry, J.A. and Anderson, T.B. 1989. Landward vergence in the lower Paleozoic Southern Uplands-Down-Longford terrane, British Isles. *Geology*, **17**, 630–633, https://doi.org/10.1130/0091-7613(1989)017<0630:LVITLP>2.3.CO;2

McEvoy, B. 1885. Kill coal-pit, Kilnaleck. Anglo-Celt, 17 January 1885, Cavan.

Meredith, W., Uguna, C.N., Snape, C.E., Carr, A.D. and Scotchman, I.C. 2019. Formation of bitumen in the Elgin–Franklin complex, Central Graben, North Sea: implications for hydrocarbon charging. *Geological Society, London, Special Publications*, **484**, 139–163, https://doi.org/10.1144/SP484-2017-344

Merriman, R.J. and Roberts, B. 2000. Low-grade metamorphism in the Scottish Southern Uplands terrane: deciphering the patterns of accretionary burial, shearing and cryptic aureoles. *Transactions of the Royal Society of Edinburgh: Earth Sciences*, **91**, 521–537, https://doi.org/10.1017/S0263593300008373

Merriman, R.J., Roberts, B., Peacor, D.R. and Hirons, S.R. 1995. Strain-related differences in the crystal growth of white mica and chlorite: a TEM and XRD study of the development of metapelitic microfabrics in the Southern Uplands thrust terrane, Scotland. *Journal of Metamorphic Geology*, **13**, 559–576, https://doi.org/10.1111/j.1525-1314.1995.tb00243.x

Moore, W.P. 1872*a*. Kilnaleck Coal Mine. Cavan Weekly News and General Advertiser, 9 August 1872, Cavan.

Moore, W.P. 1872*b*. Fuel. Cavan Weekly News and General Advertiser, 13 September 1872, Cavan

Moore, J.S. and Vrolijk, P. 1992. Fluids in accretionary prisms. *Reviews of Geophysics*, **30**, 113–135, https://doi.org/10.1029/92RG00201

Naden, J. and Caulfield, J.B.D. 1989. Fluid inclusion and isotopic studies of gold mineralization in the Southern Uplands of Scotland. *Transactions of the Institution of Mining and Metallurgy (Section B: Applied Earth Science)*, **98**, B46–B48.

Needham, D.T. 2004. Deformation in Moffat Shale detachment zones in the western part of the Scottish Southern Uplands. *Geological Magazine*, **141**, 441–453, https://doi.org/10.1017/S0016756804009203

Newell, K.D., Doveton, J.H., Merriam, D.F., Sherwood Lollar, B., Waggoner, W.M. and Magnuson, L.M. 2007. H_2-rich and hydrocarbon gas recovered in a deep Precambrian well in Northeastern Kansas. *Natural Resources Research*, **16**, 277–292, https://doi.org/10.1007/s11053-007-9052-7

Pang, X., Li, Q., Chen, J., Li, M. and Pang, H. 2014. Recovery method of original TOC and its application in source rocks at high mature-over mature stage in deep petroliferous basins. *Journal of Palaeogeography*, **16**, 769–789, https://doi.org/10.1190/ice2016-6455957.1

Parnell, J. 2022. Snowball Earth to Global Warming: coupled vanadium-carbonaceous deposits in the Cryogenian-Cambrian. *Ore Geology Reviews*, **145**, 104876, https://doi.org/10.1016/j.oregeorev.2022.104876

Parnell, J., Hole, M. and Boyce, A.J. 2015. Evidence for microbial activity in British and Irish Ordovician pillow lavas. *Geological Journal*, **50**, 497–508, https://doi.org/10.1002/gj.2562

Pereira, M., Vergani, G., Cambon, I., Reynaldi, J., Iturralde, J., Guerrero, R. and González, G. 2018. Andean deformation and its control on hydrocarbon generation, migration, and charge in the wedge-top of southern Bolivia. *In:* Zamora, G., McClay, K.R. and Ramos, V.A. (eds) *Petroleum Basins and Hydrocarbon Potential of the Andes of Peru and Bolivia*. *AAPG Memoirs*, **117**, 531–554.

Raimbourg, H., Thiéry, R. *et al.* 2017. Organic matter cracking: a source of fluid overpressure in subducting sediments. *Tectonophysics*, **721**, 254–274, https://doi.org/10.1016/j.tecto.2017.08.005

Raiswell, R. and Berner, R.A. 1987. Organic carbon losses during burial and thermal maturation of normal marine shales. *Geology*, **15**, 853–856, https://doi.org/10.1130/0091-7613(1987)15<853:OCLDBA>2.0.CO;2

Reed, J.D., Illich, H.A. and Horsfield, B. 1986. Biochemical evolutionary significance of Ordovician oils and their sources. *Organic Geochemistry*, **10**, 347–358, https://doi.org/10.1016/0146-6380(86)90035-5

Rice, S., Cuthbert, S.J. and Hursthouse, A. 2018. Tectono-magmatic controls of post-subduction gold mineralisation during late Caledonian soft continental collision in the Southern Uplands-Down-Longford Terrane, Britain and Ireland: a review. *Ore Geology Reviews*, **101**, 74–104, https://doi.org/10.1016/j.oregeorev.2018.07.016

Sanei, H. 2020. Genesis of solid bitumen. *Scientific Reports*, **10**, 15595, https://doi.org/10.1038/s41598-020-72692-2

Schito, A., Miurhead, D. and Parnell, J. 2022. Carbonaceous residues in the Southern Uplands accretionary prism of Ireland and Scotland. *Scottish Journal of Geology*, **58**, https://doi.org/10.1144/sjg2021-021

Schovsbo, N.H., Moron, J.M., Nielsen, A.T., Nicolas, G., Petersen, H.I. and Stouge, S. 2012. Thermal maturity of Lower Palaeozoic shales in North-West Europe - Calibration of proxies. 74th EAGE Conference & Exhibition, 4–7 June 2012. EAGE, Copenhagen, paper P161.

Schovsbo, N.H., Nielsen, A.T. and Gautier, D.L. 2014. The Lower Palaeozoic shale gas play in Denmark. *Geological Survey of Denmark and Greenland Bulletin*, **31**, 19–22, https://doi.org/10.34194/geusb.v31.4640

Schwangler, M., Harris, N.B. and Waldron, J.W.F. 2000. Source rock characterization and oil-to-source rock correlation of a Cambrian -Ordovician fold-and-thrust belt petroleum system, western Newfoundland. *Marine and Petroleum Geology*, **115**, 104283, https://doi.org/10.1016/j.marpetgeo.2020.104283

Steed, G.M. and Morris, G.M. 1986. Gold mineralization in Ordovician greywackes at Clontibret, Ireland. *In:* Keppie, J., Duncan, T., Boyle, R.W. and Haynes, S.J. (eds) *Turbidite-Hosted Gold Deposits*. *Geological Association of Canada Special Paper*, 67–86.

Stockey, R.G., Cole, D.B., Planavsky, N.J., Loydell, D.K., Frýda, J. and Sperling, E.A. 2020. Persistent global marine euxinia in the early Silurian. *Nature Communications*, **11**, 1804, https://doi.org/10.1038/s41467-020-15400-y

Stone, P. and Merriman, R.J. 2004. Basin thermal history favours an accretionary origin for the Southern Uplands terrane, Scottish Caledonides. *Journal of the Geological Society*, **161**, 829–836, https://doi.org/10.1144/0016-764903-170

Suzuki, N., Saito, H. and Hoshino, T. 2017. Hydrogen gas of organic origin in shales and metapelites. *International Journal of Coal Geology*, **173**, 227–236, https://doi.org/10.1016/j.coal.2017.02.014

Thickpenny, A. and Leggett, J.K. 1987. Stratigraphic distribution and palaeo-oceanographic significance of European early Palaeozoic organic-rich sediments. *Geological Society, London, Special Publications*, **26**, 231–247, https://doi.org/10.1144/GSL.SP.1987.026.01.15

Uguna, C.N., Carr, A.D., Snape, C.E., Meredith, W., Scotchman, I.C., Murray, A. and Vane, C.H. 2016. Impact of high water pressure on oil generation and maturation in Kimmeridge Clay and Monterey source rocks: implications for petroleum retention and gas generation in shale gas systems. *Marine and Petroleum Geology*, **73**, 72–85, https://doi.org/10.1016/j.marpetgeo.2016.02.028

Walters, C.C., Wang, F.C., Qian, K., Wu, C., Mennito, A.S. and Wei, Z. 2015. Petroleum alteration by thermochemical sulfate reduction – a comprehensive molecular study of aromatic hydrocarbons and polar compounds. *Geochimica et Cosmochimica Acta*, **153**, 37–71, https://doi.org/10.1016/j.gca.2014.11.021

Wang, X., Tian, H., Zhou, Q. and He, C. 2021. Origin and formation of pyrobitumen in Sinian–Cambrian reservoirs of the Anyue Gas Field in the Sichuan Basin: implications from pyrolysis experiments of different oil fractions. *Energy Fuels*, **35**, 1165–1177, https://doi.org/10.1021/acs.energyfuels.0c03263

Webb, B.C. 1983. Imbricate structure in the Ettrick area, Southern Uplands. *Scottish Journal of Geology*, **19**, 387–400, https://doi.org/10.1144/sjg19030387

Whitty, J.I. 1854. Notice of the anthracite found in the Silurian rocks, in the County of Cavan. *Journal of the Geological Society of Dublin*, **6**, 187–195.

Willner, A.P., Sepúlveda, F.A., Hervé, F., Massonne, H.-J. and Sudo, M. 2009. Conditions and timing of pumpellyite-actinolite-facies metamorphism in the early Mesozoic frontal accretionary prism of the Madre de Dios Archipelago (Latitude 50°20′S; Southern Chile). *Journal of Petrology*, **50**, 2127–2155, https://doi.org/10.1093/petrology/egp071

Xiong, Y., Jiang, W. *et al.* 2016. Formation and evolution of solid bitumen during oil cracking. *Marine and Petroleum Geology*, **78**, 70–75, https://doi.org/10.1016/j.marpetgeo.2016.09.008

Yao, L., Zhong, N. *et al.* 2021. Comparison of in-source solid bitumen with migrated sold bitumen from Ediacaran-Cambrian rocks in the Upper Yangtze region, China. *International Journal of Coal Geology*, **240**, 103748, https://doi.org/10.1016/j.coal.2021.103748

Zanella, A., Cobbold, P. and Lisandro, R. 2014. Beef veins and thrust detachments in Early Cretaceous source rocks, foothills of Magallanes-Austral Basin, southern Chile and Argentina: structural evidence for fluid overpressure during hydrocarbon maturation. *Marine and Petroleum Geology*, **55**, 250–261, https://doi.org/10.1016/j.marpetgeo.2013.10.006

Zgonnik, V. 2020. The occurrence and geoscience of natural hydrogen: a comprehensive review. *Earth-Science Reviews*, **203**, 103140, https://doi.org/10.1016/j.earscirev.2020.103140

Zhao, W., Zhang, S., Zhang, B., He, K. and Wang, X. 2017. New insight into the kinetics of deep liquid hydrocarbon cracking and its significance. *Geofluids*, **2017**, 6340986, https://doi.org/10.1155/2017/6340986